Chinese Journal of Chemical Engineering 53 (2023) 211–221

Contents lists available at ScienceDirect

Chinese Journal of Chemical Engineering

journal homepage: www.elsevier.com/locate/CJChE

Full Length Article

Pyridine terminated polyurethane dendrimer/chlorinated butyl rubber nanocomposites with excellent mechanical and damping properties

Jiacheng Chen, Jincheng Wang *, Shuhong Li, Kailing Xiang, Shiqiang Song *

College of Chemistry and Chemical Engineering, Shanghai University of Engineering Science, Shanghai 201620, China

ARTICLE INFO

Article history:
Received 17 October 2021
Received in revised form 13 February 2022
Accepted 25 February 2022
Available online 3 March 2022

Keywords:
Coordination bonds
Hydrogen bonds
Polyurethane dendrimer
Nanostructure
Polymers
Composites

ABSTRACT

Due to the special viscoelastic property, traditional rubber with high performance has been widely used in human life and production. However, it is challenging to improve the damping property without sacrificing the extensibility. In this work, a novel type of second-generation polyurethane dendrimer terminated with pyridine (G2-Py) was synthesized by using thiolactone chemistry and subsequently complexed with Zn ions. The structure and morphology of G2-Py were characterized. G2-Py-Zn^{2+} was then mixed with chlorinated butyl rubber (CIIR) by a two-roll mill. A series of CIIR/G2-Py-Zn^{2+} elastomers were obtained through vulcanization. CIIR/G2-Py-Zn^{2+} elastomers could achieve high stretchability (a strain of ~1035%), high mechanical strength (a tensile stress of 7.64 MPa). This was benefitted from the friction between G2-Py and CIIR as well as variety of non-covalent bonds provided by G2-Py-Zn^{2+}, which can dissipate energy to further improve the strength and extensibility. The coordination of Zn^{2+}-pyridine was confirmed by Fourier transform infrared spectroscopy, stress relaxation and cycle tensile test. To further investigate the morphology and damping properties of the elastomers, scanning electron microscopy and dynamic mechanical analysis were performed. CIIR-5 showed the best damping performance with higher $\tan\delta_{max}$ and wider effective damping temperatures. Therefore, this dendrimer modification technology provides wider applications for CIIR elastomers in daily life.

1. Introduction

Vibration attracts people's attention due to unpleasant noises and potential motions which may lead to fatigue, energy losses, structural damage, and degraded performance on materials [1,2]. Unfortunately, most of the materials are inherently poor in vibration damping [3]. Damping materials, which can dissipate mechanical vibration energy, become the most effective way to reduce noise and vibration [4]. Generally, the materials with high value of tanδ and wide damping temperature range are used as damping materials in practice. Particularly, rubber materials served as damping materials have the great potential for vibration reduction due to their special viscoelastic properties [5]. However, the effective damping temperature range of rubber is relatively narrow, which limits its wide applications [6].

Many efforts have been devoted to broaden the effective damping temperature range of rubber, in other words, to increase the energy dissipation of the system, such as interfacial friction [7], piezoelectric conversion [8] and introduction of non-covalent bonds [9–11]. The interfacial friction always occurs between rubber molecular chains and fillers. Gu *et al.* [12] prepared organic montmorillonite (OMMT)/natural rubber/*cis*-1,4-polybutadiene (OMMT/NR/BR) nanocomposites, and found that tanδ was shifted to higher temperature. Wang *et al.* [13] used polydopamine (PDA), silane coupling agent (KH550) and ionic liquid to modify carbon nanotubes (CNTs) as fillers into carboxylated nitrile rubber (XNBR). They found that functionalized CNTs not only inhibited their agglomeration but also modulated the interfacial interactions between CNTs and XNBR. Tang *et al.* [14] prepared a new type of OMMT which was added to chlorinated butyl rubber (CIIR). They found that OMMT endowed a positive effect on the damping and mechanical properties of CIIR nanocomposites. However, it is difficult to control the strength of the interfacial friction between matrix and filler [15]. The piezoelectric conversion is that the piezoelectric particles in the matrix convert the kinetic energy received into electrical energy and then dissipate it. Yu *et al.* [16] prepared a novel piezo-damping material. When the material was stressed, barium titanate (BT) as piezoelectric phase could generate electric charge due to mechanical deformation, while CNTs as conductive filler could dissipate the energy. This material showed good damping performance which could broad the practi-

* Corresponding author. Fax: +86 21 67791214.
E-mail addresses: wjc406@sues.edu.cn (J. Wang), songchem@126.com (S. Song).

https://doi.org/10.1016/j.cjche.2022.02.013
1004-9541/

cal application under harsh conditions. However, the realization of piezoelectric conversion requires a large amount of inorganic piezoelectric materials to be added to the rubber matrices, which may reduce the mechanical properties of the rubber material.

In recent years, reversible non-covalent bonds have been introduced into rubbers for endowing them with damping property and self-healing performance, such as coordination [17,18] and hydrogen bonds [19,20]. Lu *et al.* [19] designed a novel dendrimer which was modified by phenolic hydroxyl and amine groups (G2 PAMAM-H), as a modifier to improve the damping and mechanical properties of CIIR. Due to the multiple hydrogen bonds, the samples added G2 PAMAM-H exhibited excellent damping property. Zhang *et al.* [21] constructed a double cross-linked network consisting of covalent and sacrificeable coordination bond in nitrile butadiene rubber (NBR). They found that Zn^{2+}–CN coordination bonds presenting in rubber materials dissipated energy which may improve strength, damping property and shape memory performance simultaneously. Su *et al.* [22] prepared a novel rubber composite consisiting the oligo-phenol as organic fillers. They found that due to the strong intermolecular interactions between surface functional groups of organic fillers and the matrix, the temperature range of sample was expanded to 100.28 °C with $\tan\delta > 0.3$ compared to the pure sample.

Inspired by the energy dissipation mechanism of coordination and hydrogen bonds, a dendrimer was designed in this study to combine these two bonds together to improve the damping properties of CIIR. Dendrimer, which owned regular structure and molecular connection like a divergent tree crown, is a very particular class of macromolecules among all types of polymers [23]. Due to the special advantages of controllable and precise molecular structure, highly branched structure and dense surface functional groups, dendrimer attracted more attention from scientists on agriculture [24], drug delivery [25,26], and catalysis [27,28]. In this study, we chose dendrimer as a rubber modifier because of its dense external functional groups and controllable molecular design.

We aimed to improve the damping properties of CIIR by introducing two non-covalent bonds. First, a second-generation pyridine-terminated polyurethane (G2-Py) was obtained by using the thiolactone chemistry [29]. Next, Zn ions were provided by zinc chloride, and coordinated with pyridine on G2-Py. Then, G2-Py-Zn^{2+} were mixed into CIIR matrix, and CIIR chains were vulcanized by sulfur. The tensile properties, dynamic mechanical properties and morphology were studied to verify the effect of the introduction of G2-Py-Zn^{2+} to CIIR matrix. We guessed that the introduction of hydrogen bonds and coordination bonds (Zn^{2+}-pyridine) may dissipate more energy while the elastomers were stressed.

2. Material and Methods

2.1. Materials

Triphosgene (99%), DL-homocysteine thiolactone hydrochloride (99%), dibutyltin dilaurate (DBTL, 95%), propanolamine (99%), 3-aminopyridine (99%) and hydroxyethyl acrylate (98%) were provided by the Adamas series of Shanghai Titan Scientific Co. Ltd. (Shanghai, China). Dichloromethane (99.5%), pyridine (99.5%), hydrochloric acid (HCl, 36%–38%), magnesium sulfate ($MgSO_4$, 98%), triethanolamine (99%), zinc chloride (98%), tetrahydrofuran (THF, 99.5%), ethyl acetate (99.5%), chloroform (99%), hexane (97%) and diethyl ether (99.5%) were obtained from the Greagent series of Shanghai Titan Scientific Co. Ltd. (Shanghai, China). Chlorinated butyl rubber (CIIR, *Mn* = 255,800, PDI = 1.72 (polydispersity index), Exxon 1066) was purchased from Exxon Mobil Chemical Industry Company (Shanghai, China). Dibenzothiazole disulfide, magnesium oxide, tetramethyl thiuram disulfide, stearic acid, sulfur, and zinc oxide as rubber additives were commercial chemicals from market (Shanghai, China).

2.2. Preparation of G2-Py-Zn^{2+}

The reaction scheme of G2-Py was shown in Fig. 1.

2.2.1. Synthesis of α-isocyanato-γ-thiolactone [30]

The synthesis of α-isocyanato-γ-thiolactone, as shown in Fig. 1 (a), was performed according to the procedure described in literature [30]. Triphosgene (12.5 g, 42 mmol) was dissolved in 100 ml cold CH_2Cl_2, and 125 ml CH_2Cl_2 was added after DL-homocysteine thiolactone hydrochloride (18.5 g, 12 mmol) was slowly poured into reaction mixture by funnel. Next, dry pyridine (35 ml) was added dropwise to the reaction mixture. The reaction mixture was kept in an ice-bath for 1 h, and was stirred for an additional 4 h at room temperature. The reaction mixture was directly filtered in a Buchner funnel and was washed with 2 mol·L^{-1} HCl solution (250 ml), saturated brine (250 ml) and ice water (250 ml). Then, $MgSO_4$ was added into the organic phase to remove residual water. After evaporation of the CH_2Cl_2, the residue was purified by vacuum distillation, and transparent oil was obtained.

2.2.2. Preparation of thiolactone end-capped triethanolamine (G0-TL) and G1 (G1-TL)

The reaction of α-isocyanato-γ-thiolactone with triethanolamine was performed according to the previous literature [29–31]. Briefly, triethanolamine (1.788 g, 0.012 mol, 1 equivalent (eq)) was dissolved in anhydrous chloroform. Fresh α-isocyanato-γ-thiolactone (5.663 g, 0.0396 mol, 1.1 eq per hydroxyl group) and dibutyltin dilaureate (DBTL,catalyst) was added to the reaction mixture under N_2 atmosphere. The reaction was conducted at 70 °C for 24 h. After precipitation in cold hexane (one time) and cold diethyl ether (two time), the light-yellow residue was dried in a vacuum oven at 60 °C for 12 h to prepare thiolactone end-capped triethanolamine (G0-TL). G1-TL was also obtained according to this procedure.

2.2.3. Preparation of G1 and G2-Py

The aminolysis and thiol-acrylate reaction was conducted according to the previous literature [29–31]. Briefly, TEA-TL (5.78 g, 0.01 mol, 1 eq) was dissolved in chloroform. Propanolamine (11.25 g, 0.15 mol, 5 eq per TL function) and 2-hydroxyethyl acrylate (34.8 g, 10 eq per TL function) was added to the solution. The reaction was stirred at ambient temperature for 24 h. Afterwards, the residue was precipitated in diethyl ether and washed with ethyl acetate (two times). Finally, after drying under vacuum overnight, the target product G1 was obtained. G2-Py was also obtained according to this procedure. However, propanolamine was replaced by aminopyridine.

2.2.4. Metal incorporation

The scheme of incorporation of Zn^{2+} and pydrine was shown in Fig. 1(c). Specifically, G2-Py (3.27 g, 1 mmol) was dissolved in 10 ml THF, and $ZnCl_2$ (0.2 g, 1.5 mmol) was added to the solution. After stirring at room temperature for 4 h, the solution was kept in a fume cupboard to evaporate the solvent. The sample, G2-Py-Zn^{2+}, was further dried under vacuum overnight to ensure complete removal of solvents.

2.3. Preparation of CIIR/G2-Py-Zn^{2+} elastomers

Stearic acid, magnesium oxide, dibenzothiazole disulfide, tetramethylthiuram disulfide, G2-Py-Zn^{2+}, zinc oxide and sulfur were successively compounded with CIIR on a two-roll mill within

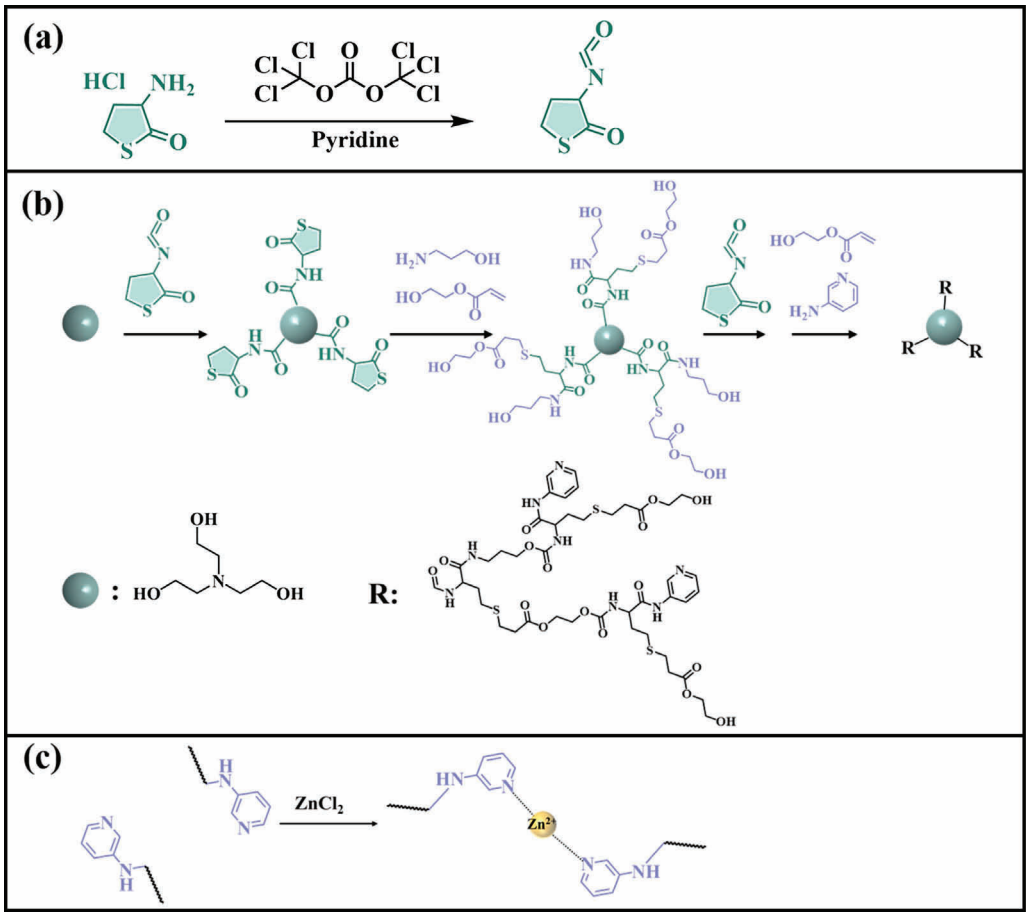

Fig. 1. (a) Synthesis of α-isocyanato-γ-thiolactone. (b) The entire reaction step for the synthesis of G2-Py. (c) Scheme of metal incorporation.

30 min. The proportions of these additives were listed in Table 1. Finally, the compounds were compressed for the curing time determined from the curing curve. A series of CIIR/G2-Py-Zn^{2+} elastomers were obtained named CIIR-*x*, which refered to that *x* phr (parts per one hundred parts of CIIR) of G2-Py-Zn^{2+} was added in CIIR. For comparison, the composites named CIIR-5-0 was prepared by adding 5 phr G2-Py.

2.4. Characterizations

The morphology and microstructure of G2-Py were observed by transmission electron microscopy (TEM, JEOL JEM-F200, Japan). The infrared spectra of G2-Py and G2-Py-Zn^{2+} were characterized by Fourier transform infrared spectroscopy (FTIR, AVATAR 370, Nicolet, USA). The CIIR-5 was heated from 25 to 200 °C at 10 °C·min^{-1}, and the temperature-dependent FTIR spectra were collected at different temperatures. The structure and chemical composition of each step of dendrimer were characterized by ^{1}H and ^{13}C nuclear magnetic resonance spectrum (NMR) (Bruker Avance-III 400 MHz, Switzerland) and matrix-assisted laser desorption/ionization time of flight mass spectrometry (MALDI-TOF-MS, Voyager DE-STR, USA). The tensile properties of CIIR/G2-Py-Zn^{2+} elastomers were measured by tensile tester (GT-TCS-2000, Gotech Testing Machines Co., Ltd., China) using an extension rate of 1000 mm·min^{-1} at room temperature. The fracture energy (W) is defined as the area surrounded by the stress (σ)–strain (ε) curves and calculated using Eq. (1) as follows [32]:

$$W = \int_0^{\varepsilon} \sigma(\varepsilon) \mathrm{d}\varepsilon \tag{1}$$

The loading and unloading test of CIIR composites was tested with an extension rate of 250 mm·min^{-1} at room temperature. In each cycle, the sample was stretched to a strain of 500%, and then relaxed at room temperature for a certain waiting time (0, 30, 120 and 300 s) before the subsequent loading process. The stress relaxation test of ealstomers was performed on a HY-940FS (Taiwan, China) instrument with an extension rate of 100 mm·min^{-1} at room temperature. The sample was stretched to a strain of 100% and held for 1200 s at room temperature. The dynamic mechanical analysis (DMA) was performed using a dynamic momechanical analyzer (DMA, TA Q800, USA). The sample was measured for storage modulus (E'), loss modulus (E'') and loss factor (tanδ) from –80 to 100 °C with a temperature increase rate of 3 °C·min^{-1} under liquid nitrogen. The morphology of elastomers was observed using scanning electron microscopy (SEM, ZEISS Gemini 300, Germany) and energy-dispersive spectroscopy (EDS). The cross-linking density (n) of samples were measured by the equilibrium swelling experiments. Samples were weighed (m_0) and swollen in toluene at room temperature for 3 days. After removing toluene from the

Table 1
Composition of different CIIR elastomers

Components	Parts per hundred of rubber (phr)
CIIR	100
Stearic acid	1
Magnesium oxide	0.15
Dibenzothiazole disulfide	2
Tetramethylthiuram disulfide	1.5
Zinc oxide	5
Sulfur	1
G2-Py-Zn^{2+}	1, 3, 5, 7, 10

surface, samples were weighed (m_1) and dried in an oven at 70 °C for 3 days until constant mass (m_2). The cross-linking density (n) was calculated according to the Flory–Rehner equation [33,34]

$$n = \frac{-[\ln(1-\phi_r)+\phi_r+\chi\phi_r^2]}{V_o(\phi_r^{1/3}-\phi_r/2)} \quad (2)$$

where χ is Flory–Huggins polymer–solvent interaction term (0.393 for toluene); V_0 is mole volume of toluene (106.2 $cm^3 \cdot mol^{-1}$); ϕ_r is the volume fraction of rubber swollen was calculated by Eq. (3):

$$\phi_r = \frac{m_2/\rho_r}{m_2/\rho_r + (m_1-m_2)\rho_s} \quad (3)$$

where ρ_s and ρ_r are the tolune and rubber density, respectively.

3. Results and Discussion

3.1. Preparation analysis of CIIR/G2-Py-Zn^{2+} elastomers

G2-Py was synthesized by using thiolactone chemistry. Specifically, triethanolamine was modified by thiolactone with isocyanate functional group. The thiolactone could undergo efficient ammonolysis, and the resulting thiol could react with the double bond of the acrylate derivative. The obtained G2-Py was subsequently complexed with Zn^{2+} ions. To achieve homogeneous blends, CIIR was first plasticized to disperse G2-Py into the interior of the CIIR. The CIIR/G2-Py blends were molded and cross-linked by compressing them between two metal molds at 150 °C. A series of CIIR/G2-Py-Zn^{2+} elastomers were obtained, as shown in Fig. 2(a). The proposed structure of CIIR/G2-Py-Zn^{2+} elastomers were shown schematically in Fig. 2(b), wherein the elastomers showed excellent ability to dissipate energy during stretching.

3.2. Analysis of the synthesized G2-Py and G2-Py-Zn^{2+}

G2-Py was synthesized through the thiolactone aminolysis and thiol-ccrylate reaction. The structure of the samples in each step was characterized by ^{1}H NMR (Fig. 3). The characteristic shifts at 3.30, 2.64 and 2.08 in Fig. 3(a) can be attributed to S—CH_2—CH_2 and CH_2—CH_2—CH in the thiolactone ring, respectively [30,35]. The reaction of α-isocyanato-γ-thiolactone and hydroxyl proved to be successful due to the appearance of the signal for the thiolactone ring in Fig. 3(b) and (d). Meanwhile, the characteristic peaks at 3.39 and 3.56 in the Fig. 3(c) can be assigned to OH—CH_2—CH_2 in the G1 chains. However, such characteristic shift was biased towards the low field about 4.29 as shown in Fig. 3(d) due to the strong electronegativity of the carbonyl group, which proved the successful reaction between hydroxyl and isocyanate. The aminolysis was demonstrated to be achieved by the signal disappearance of the thiolactone ring in Fig. 3(c) and (e). Meanwhile, Fig. 3(f) presented ^{13}C NMR of G2-Py. The characteristic shifts at 148.8, 145.2 and 137.4 may be assigned to C—*C*H—CH, CH—*C*H—N and N—*C*H—C in pyridine ring, respectively, confirming the thiolactone ring of G1-TL was successfully opened by 3-aminopyridine [36].

MALDI-TOF-MS was performed on the obtained G2-Py to confirm the analysis results of ^{1}H NMR and ^{13}C NMR. Fig. 4(a) showed that the molecular weight of G2-Py was mainly distributed around 3000. The average molecular weight of G2-Py was about 3272, while the peak at 3295 was due to the added sodium salt during the test.

FTIR was performed to confirm the interaction between Zn^{2+} and pyridine, and the spectra of G2-Py and G2-Py-Zn^{2+} were shown in Fig. 4(b). In the case of G2-Py, the absorption peaks at 1712 and 1586 cm^{-1} were assigned to stretching of urethane carbonyl (C=O) [37] and the bending vibrations of —C=N in the free pyridine group [38], respectively. After adding Zn^{2+} to G2-Py, a stronger peak was observed at 1636 cm^{-1}, while the absorption peak at 1586 cm^{-1} was offset to 1580 cm^{-1}. The absorption of 1636 cm^{-1} was due to the —C≡N vibration mode of the coordination bonded pyridine groups, confirming the coordination of pyridine with Zn^{2+} [39–41]. Moreover, the absorption peak of G2-Py-Zn^{2+} at 1580 cm^{-1} associated with the free pyridine was reduced. Interestingly, urethane carbonyl group (C=O) at 1712 cm^{-1} remained unchanged, indicating that Zn^{2+} was only coordinated to pyridine ligand, not to urethane groups.

TEM images (Fig. 4(c) and (d)) showed that due to the dispersion in water and ethanol, the agglomeration of the G2-Py can be clearly seen. G2-Py presented a spherical appearance with a diameter of about 10 nm. However, the size of agglomerated particles can reach about 2 μm. It can be guessed that many hydrogen bonds were formed inside the agglomeration structure.

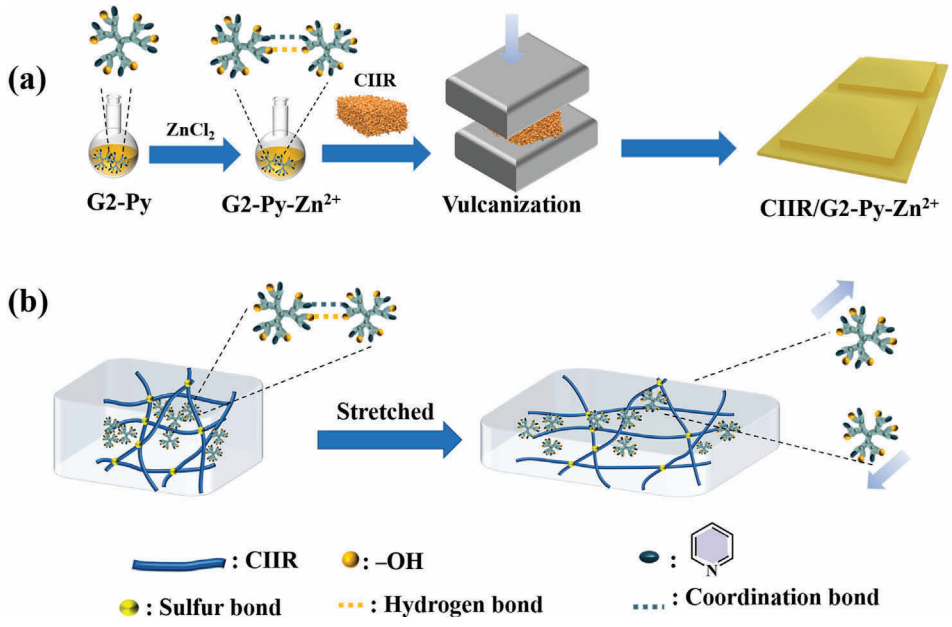

Fig. 2. (a) Schematic illustration of preparation process of CIIR/G2-Py-Zn^{2+} elastomers. (b) Schematic structure and proposed mechanism during stretching of CIIR/G2-Py-Zn^{2+} elastomers.

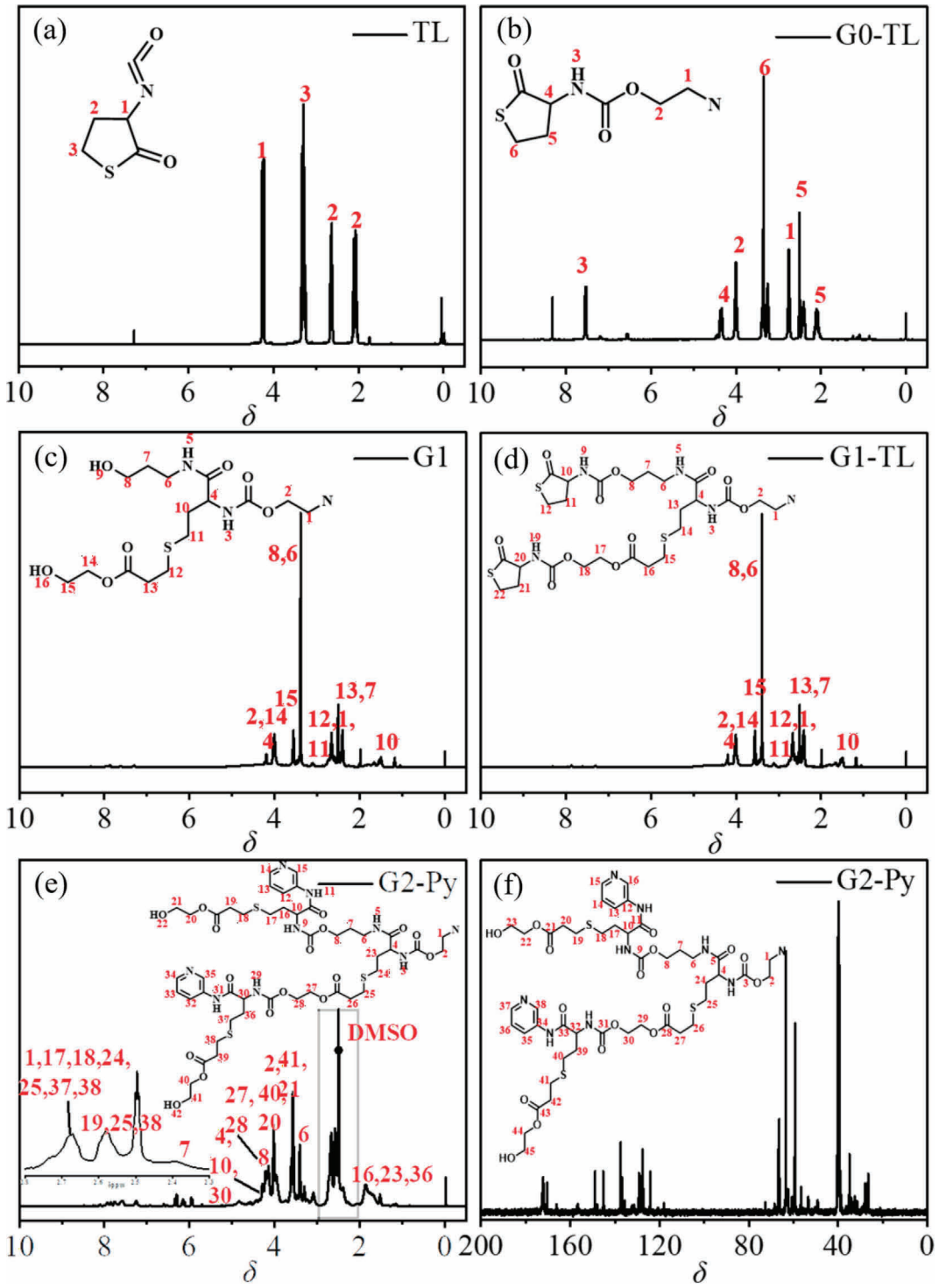

Fig. 3. ^{1}H NMR of (a) TL, (b) G0-TL, (c) G1, (d) G1-TL, (e) G2-Py, ^{13}C NMR of (f) G2-Py.

3.3. Tensile properties of CIIR/G2-Py-Zn^{2+} elastomers

The typical stress–strain curves of CIIR/G2-Py-Zn^{2+} elastomers were shown in Fig. 5. With the addition of G2-Py-Zn^{2+}, the tensile strength of the elastomers was significantly improved without sacrificing the extensibility (Fig. 5(a)). The introduction of coordination and hydrogen bonds gave rise to notable improvements in tensile stress and tensile strain at break of elastomer when adding 1–5 phr G2-Py-Zn^{2+}. Among them, the tensile stress and tensile strain at break of CIIR-5 were 1035% and 7.64 MPa, respectively, which showed the highest elongation and the highest tensile strength. Besides, CIIR-5 was chosen for further investigation due to its excellent strength and stretchability. When 7 and 10 phr G2-Py-Zn^{2+} were added, the mechanical properties of the elastomer became worse. This may be attributed to the stress concentration caused by agglomeration of too many polar molecules in the elastomer. It was inferred that G2-Py-Zn^{2+} was added to the CIIR matrix as a polar modifier.

The fracture energy (area of the stress–strain curve) of CIIR/G2-Py-Zn^{2+} was shown in Fig. 5(b). It was obvious that the fracture energy of CIIR was improved with the introduction of G2-Py-Zn^{2+}. Compared to the pure CIIR, the fracture energy of CIIR-5

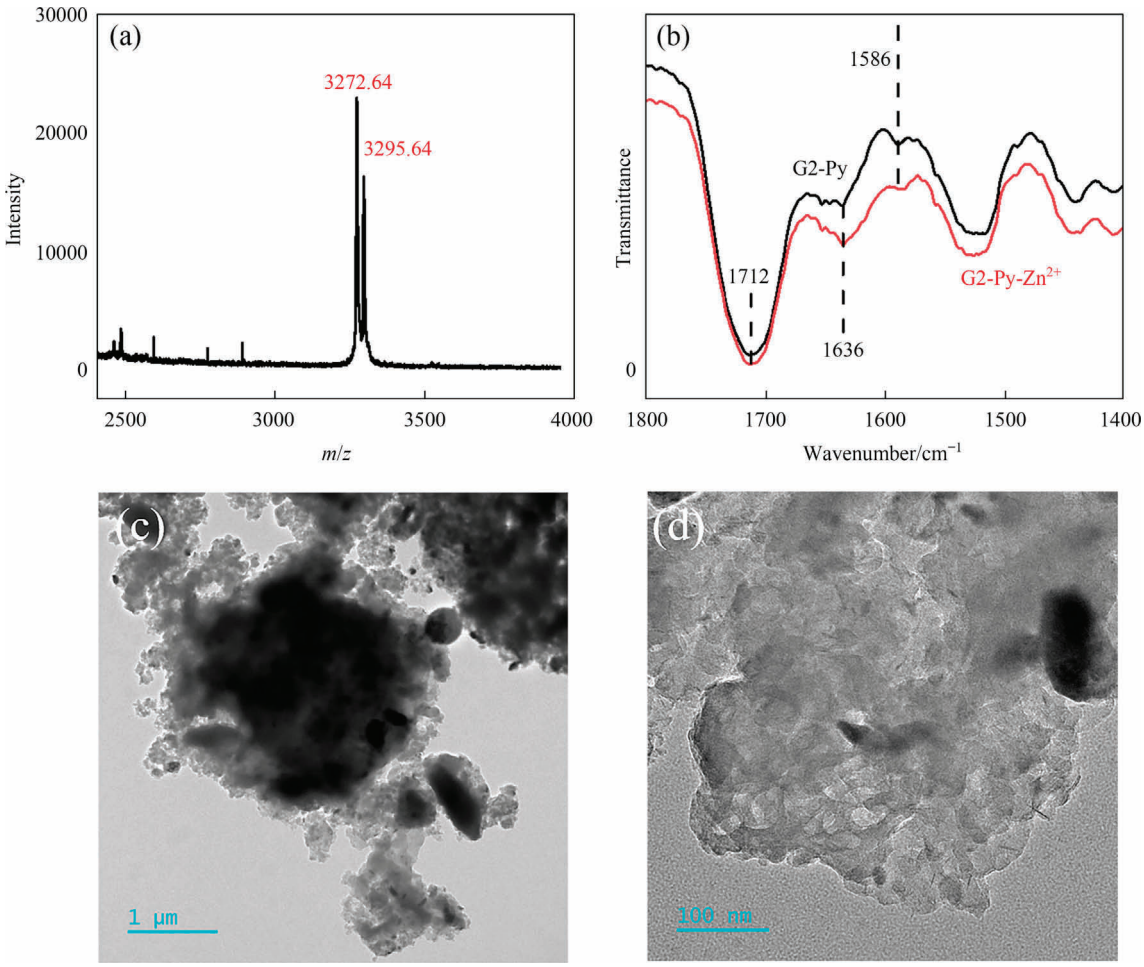

Fig. 4. (a) MALDI-TOF-MS of G2-Py, (b) FTIR of G2-Py and G2-Py-Zn^{2+}, (c) and (d) TEM images of G2-Py.

was improved by 100%, which corresponded to the higher stress and strain in stress–strain curves (Fig. 5(a)). It was critical but challenging to simultaneously improve the strength and extensibility of rubber materials, for the reason that the improved strength conflicted with enhanced extensibility. The flexible rubber networks could withstand large deformations but exhibit shallow stress responses, while restricted or rigid rubber networks showed greater strength but failed in short extensions [39]. In the obtained elastomers, the covalent network imparted elasticity and kept the permanent shape, while the coordination and hydrogen bonds served as dynamic roles to dissipate energy to increase the strength and extensibility. Due to the weak polar molecular chains of CIIR matrix and the strong polar functional groups of the G2-Py, the compatibility of the dendrimer in the rubber matrix was poor. Therefore, the dendrimer may present a sea-island structure in the matrix. During the stretching process, the CIIR molecular chains tended to straighten from curling, and the G2-Py-Zn^{2+} dispersed in it were squeezed and sheared. Simultaneously, not only the friction between the G2-Py and the CIIR molecular chains, but also the reversible non-covalent bonds between the G2-Py-Zn^{2+} can dissipate energy [19,39].

In order to study the effect of coordination bonds between Zn^{2+} and pyridine on the mechanical properties of elastomers, the CIIR-5-0 was prepared. Comparing CIIR-5-0 and CIIR-5, with the introduction of coordination bonds, the tensile strength was increased from 5.39 to 7.64 MPa, while their elongations at break were similar (Fig. 5(a)). It can be clearly seen that the introduction of coordination bonds can keep the elongation at break of the elastomer, but significantly increased the tensile strength of the elastomer. This may be because the strength of the coordination bonds were greater than that of the hydrogen bonds, and the coordination bonds may dissipate more energy during stretching.

To verify the sacrificial and reversible bonds in the elastomers, the cyclic tensile tests were performed on CIIR-5. As shown in Fig. 5 (c), for the first cycle without waiting time, the hysteresis loop was much smaller. When the elastomer was allowed to relax for a certain time before the next cycle, the loading curve gradually returned to the first as the waiting time increased. This was possibly because hydrogen bonds and coordination bonds cannot fully regenerate in the time scale, which may lead to that fewer coordination bonds and hydrogen bonds can participate in the next energy dissipation [42].

In order to monitor the cross-linking network of the elastomer, the optimal vulcanization time (t_{90}) as well as the cross-linking density were listed (Table 2). As the parts of G2-Py-Zn^{2+} were increased, the optimal vulcanization time of the composites gradually increased and the vulcanization rate decreased. It may be due to the fact that G2-Py-Zn^{2+} were oligomers, and they had no reactive groups which can co-vulcanize with CIIR. Meanwhile, they hindered the cross-linking reaction of rubber molecular chains [43]. In order to further study the degree of vulcanization of the elastomer, the equilibrium swelling experiments were performed to characterize the cross-linking density, as shown in Table 2. We found that the addition of G2-Py-Zn^{2+} resulted in an increase in cross-linking density, which was consistent with the vulcanization

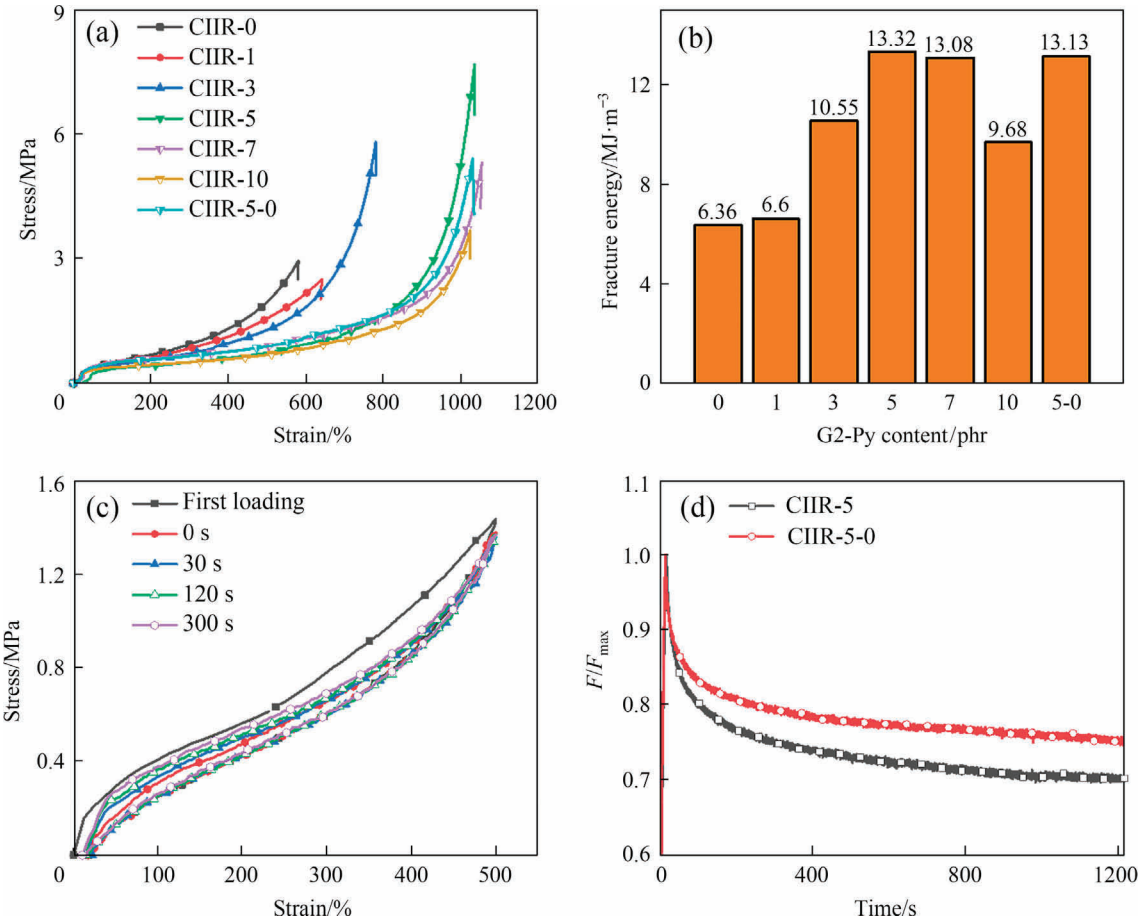

Fig. 5. (a) Typical stress–strain curves of CIIR/G2-Py-Zn^{2+} elastomers with different contents of G2-Py-Zn^{2+}. (b) Fracture energy of CIIR/G2-Py-Zn^{2+} elastomers with different contents of G2-Py-Zn^{2+}. (c) Cyclic stress–strain curves of CIIR-5 with 500% strain for different waiting time at a tensile rate of 250 mm·min^{-1}. (d) Stress relaxation of CIIR-5 and CIIR-5-0 was measured at 100% strain.

time. It can be seen that the cross-linking density of CIIR-10 was significantly greater than that of CIIR-5, but the tensile strength was not increased.

To further study the dynamic characteristics of the coordination bonds as sacrificial bonds, the stress relaxation at room temperature for CIIR-5 and CIIR-5-0 were shown in Fig. 5(d). These two samples were stretched to 100% strain at a tensile rate of 250 mm·min^{-1}, and maintained for 1200 s. Compared with CIIR-5-0, the stress for CIIR-5 relaxed much faster, which confirmed that the coordination bonds suffered from dissociation under load [39]. After a significant drop, the force in both samples remained constant over time, which was attributed to the ability of the covalently cross-linked network in the rubber to maintain the stress [44]. These findings demonstrated that during the stretching process, the hydrogen and coordination bonds between the G2-Py-Zn^{2+} may dissipate energy in a sacrificial and reversible manner, which improved the mechanical properties of elastomers.

Table 2
Cross-linking density and vulcanization parameters of CIIR/G2-Py-Zn^{2+} elastomers

Sample	Cross-linking density/10^{-4} mol·cm^{-3}	t_{90}/s
CIIR-0	2.36	534
CIIR-1	2.67	844
CIIR-3	2.85	915
CIIR-5	3.51	1291
CIIR-7	4.47	1381
CIIR-10	5.15	1418
CIIR-5-0	3.89	1249

3.4. Dynamic mechanical properties CIIR/G2-Py-Zn^{2+} elastomers

The storage modulus, loss modulus, and loss tangent (tanδ) of CIIR/G2-Py-Zn^{2+} elastomers were shown in Fig. 6. As presented in Fig. 6(a), the storage modulus (E') was increased by adding G2-Py-Zn^{2+} into the matrix. However, it can be clearly seen that the storage modulus did not increase linearly with the increasing content of G2-Py-Zn^{2+} at low temperatures, where the storage modulus of CIIR-5 was the largest and CIIR-1 was greater than CIIR-10. The hydrogen bonds and coordination bonds were formed by G2-Py-Zn^{2+}, thus leading to the increase of E' [39]. The loss modulus (E'') of neat CIIR showed a peak at –55.42 °C, which shifted toward higher temperature and higher modulus as the addition of G2-Py-Zn^{2+} (Fig. 6(b)). The temperature after the peak was the glass-rubber transition temperature range of CIIR (tanδ > 0.3, Fig. 6(c)), and the molecular segments of CIIR started to move at that time. At this time, the G2-Py-Zn^{2+} started to be squeezed by CIIR segments, which consumed a certain amount of energy. Tanδ_{max} of CIIR was a lag behind the peak of loss modulus (–29.84 °C, Fig. 6(c)) about 25 °C. Such phenomenon was interpreted in terms of the effective chain packing [45].

The tanδ–temperature curves of CIIR elastomers with different G2-Py-Zn^{2+} dosages at 1 Hz were shown in Fig. 6(c). The incorporation of coordination bonds and hydrogen bonds gave rise to nota-

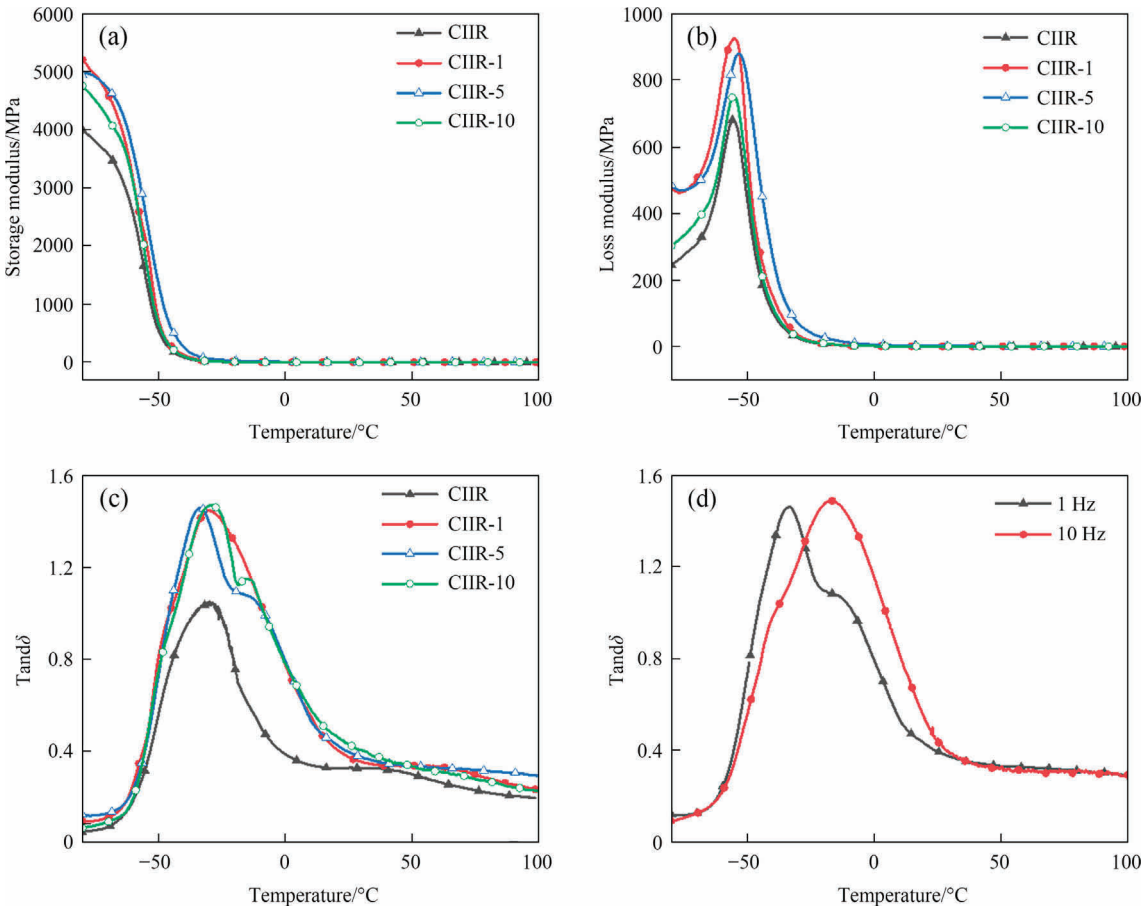

Fig. 6. (a) Storage modulus *E′* of CIIR-*x* at 1 Hz. (b) Loss modulus *E″* of CIIR-*x* at 1 Hz. (c) Damping curves of CIIR-*x* at 1 Hz. (d) Damping curves of CIIR-5 at different frequencies, 1 and 10 Hz.

ble improvements in the peak of tanδ. Specifically, the tanδ_{max} of the elastomers increased from 1.04 to 1.47 by adding different dosages of G2-Py-Zn^{2+}. The effective damping temperature range (tanδ > 0.3) was also an index to evaluate damping properties of rubber materials. Specifically, the damping temperature range of pure CIIR was 104 °C (−55 to 49 °C) and the range of CIIR-5 was 149 °C, which was increased by 143% compared to pure CIIR. The same phenomenon occurred for the CIIR-1 and CIIR-10. It can be clearly seen in Fig. 6(c) that a peak of tanδ appeared near −14 °C, which was not the peak of CIIR (near −29 °C). This was attributed to the incompatibility of CIIR and G2-Py. In summary, the effective damping area moved towards higher temperature and higher tanδ, which expanded the practical applications. It may be because G2-Py had no active groups to react with sulfur so that they cannot covulcanize with CIIR [46]. G2-Py molecular chains may generate friction effect with CIIR chains. Meanwhile, the coordination bonds and hydrogen bonds among G2-Py-Zn^{2+} dissipated energy in a reversible manner, which aggravated the hysteresis phenomenon of the material.

Since the frequency of vibration in actual use was rarely 1 Hz, the DMA curve of CIIR-5 at 10 Hz was measured (Fig. 6(d)). It was obvious that CIIR-5 displayed a wide damping temperature range (>100 °C) at 1 Hz and 10 Hz. Tanδ_{max} and the corresponding temperature increased with the increase of frequency. This may be because the hysteresis effect of the molecular chains became much more serious as the frequency increased, which improved the internal friction between the molecular chains [46]. Briefly, the damping properties of the elastomers were improved with the addition of G2-Py-Zn^{2+}.

3.5. Morphology observation of CIIR/G2-Py-Zn^{2+} elastomers

The morphology of fracture surface for CIIR elastomers was observed with SEM as presented in Fig. 7(a)–(d). The images of pure CIIR showed a single-phase morphology, with small particles on the surface of the substrate and no obvious particle agglomeration (Fig. 7(a)). These particles may be originated from rubber additives used in rubber vulcanization. After adding G2-Py-Zn^{2+}, the images showed a clear sea-island structure (Fig. 7(b)–(d)), in which the continuous phase of the 'sea' was CIIR and the 'island' was G2-Py-Zn^{2+}. The incompatible particles were dispersed on the surface of the CIIR section, and the diameter of particles was about 10–20 μm. As the dosages of G2-Py-Zn^{2+} increased, more particles can be seen in CIIR composites, especially CIIR-5. Moreover, after adding 10 phr of G2-Py-Zn^{2+}, holes can be seen on the rubber surface, which may be due to exfoliation of the particles.

The internal morphology of CIIR elastomers was further studied by SEM and EDS, which provided specific distribution information of the elements on the surface of the composites. As shown in Fig. 7(e) and (f), the elements Cl, O and S were detected. Fig. 7(e1) and (f1) showed the mapping analysis of the cross-section of CIIR-0 and CIIR-5. In Fig. 7(e1), the elements Cl, S and O were uniformly distributed on the CIIR-0 section, which was consistent with the single-phase morphology observed in Fig. 7(a). After adding 5 phr of G2-Py-Zn^{2+}, the distribution of elements became uneven. This may be because the G2-Py contained many O and S elements, and was lack of Cl elements. Compared to Fig. 7(e1)(Cl), there were clear shadings in Fig. 7(f1)(Cl), which corresponded to the incompatible particles in Fig. 7(f1). This showed that the G2-Py molecular

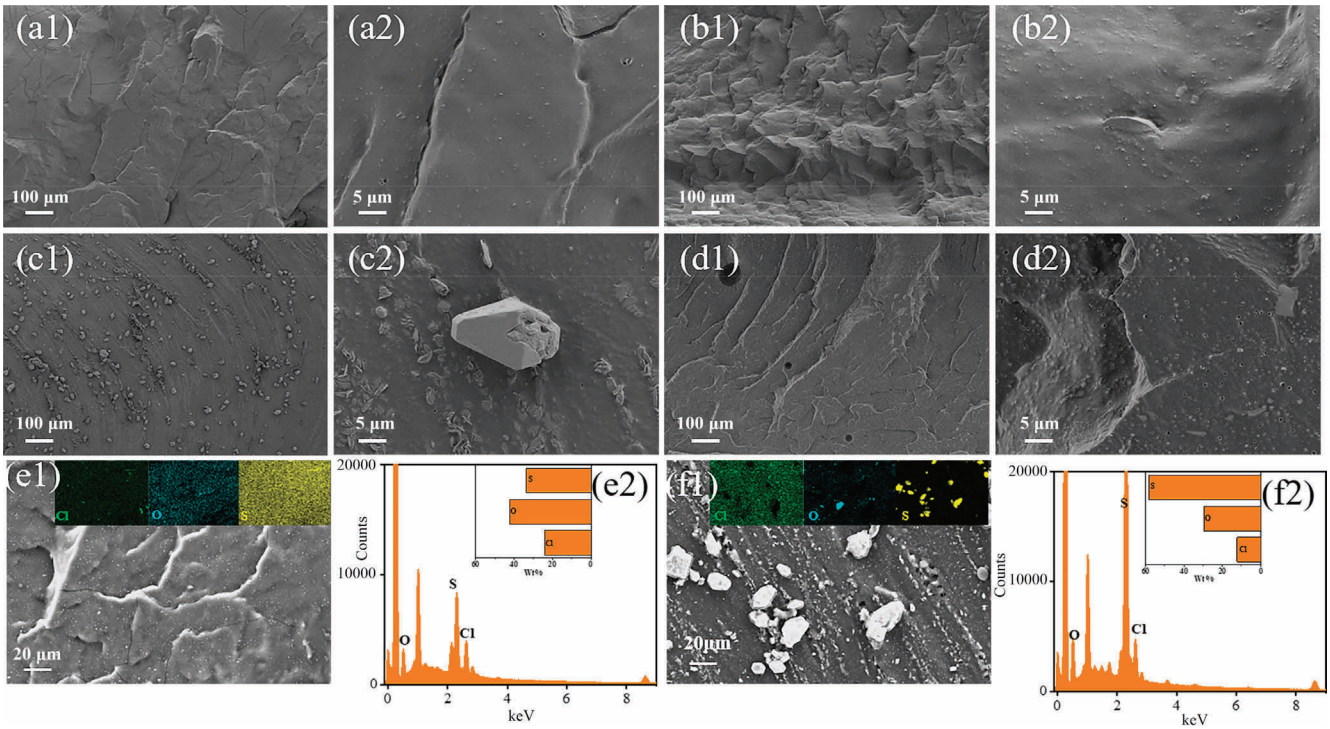

Fig. 7. SEM images of (a1–a2) pure CIIR, (b1–b2) CIIR-1, (c1–c2) CIIR-5, (d1–d2) CIIR-10. SEM–EDS mapping of (e1) pure CIIR, (f1) CIIR-5, Cl, O, S were detected. Element content of (e2) pure CIIR, (f2) CIIR-5.

chains were not physically entangled with the CIIR molecular chains. The uneven distribution of O and S elements in Fig. 7(f1)(O) and (f1)(S) were caused by a large number of carbonyl groups, ether bonds and carbon–sulfur bonds in G2-Py. The elements contents of CIIR-0 and CIIR-5 were shown in Fig. 7(e2) and (f2), respectively. Compared to CIIR, as the introduction of G2-Py-Zn^{2+}, the contents of S was sharply increased while the contents of Cl was decreased due to the incompatibility. It was obvious that the addition of G2-Py-Zn^{2+} had a great influence on the distribution of elements of CIIR. It can be inferred that, due to incompatibility, G2-Py-Zn^{2+} was agglomerated into irregular particles and dispersed evenly in the CIIR matrix.

3.6. Toughening and damping mechanisms of CIIR/G2-Py-Zn^{2+} elastomers

G2-Py possessed a lot of polar groups such as pyridine, urethane, hydroxyl and amide groups, while CIIR matrix owned only the polar atoms of Cl in the branched chains with non-polar main chains. Therefore, the compatibility between G2-Py and CIIR was poor, corresponding to the new peak of tanδ in Fig. 6(c) and the obvious particles in SEM images (Fig. 7). Furthermore, G2-Py had no active groups to react with sulfur, so that they cannot covulcanize with CIIR. The poor compatibility may lead to high internal friction, which can convert more mechanical energy into thermal energy [12,47]. It can be inferred that G2-Py-Zn^{2+} agglomerated into irregular particles distributed in the CIIR matrix (Fig. 7), which may generate friction effect with CIIR chains [46].

The temperature-dependent FTIR was performed to characterize the hydrogen bonds in the sample, as shown in Fig. 8. G2-Py theoretically possesses structures such as carbonyl and hydroxyl groups, which can form hydrogen bonds. We enlarged the FTIR spectra from 3600 to 3000 cm^{-1} and from 1700 to 1550 cm^{-1}. The absorption peaks of hydroxyl and carbonyl groups can be seen in the range of 3200–3500 cm^{-1} and 1650–1550 cm^{-1} at room temperature in Fig. 8(a) and (b), respectively, which proved the formation of hydrogen bonds from interactions among these polar groups [48]. However, as the temperature increased, the absorption peak of the hydroxyl group showed a blue shift from 3332 to 3347 cm^{-1}. Also, the absorption peak of the carbonyl group shifted from 1620 to 1627 cm^{-1}. These results indicated that the associated hydrogen bonds gradually dissociated with the increase of temperature [49].

When CIIR/G2-Py-Zn^{2+} elastomers were stressed, the curled chains of CIIR tended to be straight. The motion of the CIIR chains may squeeze and shear the particles. Meanwhile, due to the hydrogen bonds from carbonyl and hydroxyl and coordination bonds between Zn^{2+} and pyridine, the G2-Py-Zn^{2+} can dissipate energy in a reversible manner. Thus, when the samples were subjected to external forces, more energy can be dissipated by G2-Py-Zn^{2+}, which may lead to high toughening and damping properties of CIIR/ G2-Py-Zn^{2+} macroscopically.

4. Conclusions

In summary, G2-Py was obtained by using thiolactone chemistry to introduce hydroxyl groups and pyridine groups simultaneously, which aimed to form the hydrogen bonds and coordination bonds, respectively. Then, G2-Py-Zn^{2+} was added into CIIR matrix as polar modifier, with excellent mechanical properties. In addition, the morphology of CIIR/G2-Py-Zn^{2+} showed the compatibility of G2-Py and CIIR was poor, which was also verified by the DMA test. G2-Py-Zn^{2+} agglomerated into irregular particles and dispersed in the CIIR matrix. The introduction of G2-Py-Zn^{2+} endowed the polymeric elastomer with a tensile strength of 7.64 MPa and good stretchability (a strain of ~1030%). Meanwhile, the damping property of the elastomer was improved with a high value of $\tan\delta_{max}$ (1.47) and a wide effective temperature range (149 °C). The key to achieve these properties was the synergistic effect of double dynamic bonds including reversible Zn^{2+}-pyridine coordination bonds and hydrogen bonds. Therefore, this study provides a novel and effective approach to the design of damping materials,

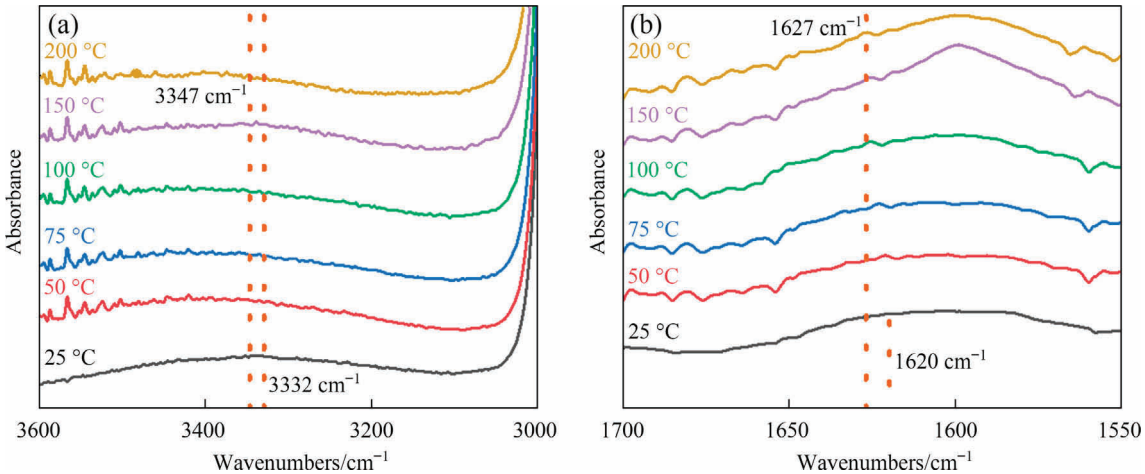

Fig. 8. Temperature-dependent FTIR spectra of CIIR-5: (a) from 3600 cm^{-1} to 3000 cm^{-1}; (b) from 1700 cm^{-1} to 1550 cm^{-1}.

which may be used as structural materials in high vibration machine.

Declaration of Competing Interest

The authors declare that they have no known competing financial interests or personal relationships that could have appeared to influence the work reported in this paper.

Acknowledgements

This work was financially supported by the National Natural Science Fundation of China ((51873103), Capacity Building Project of Some Local Colleges and Universities in Shanghai (17030501200), Talent Program of Shanghai University of Engineering Science (2017RC422017) and Postgraduate Research and Innovation Project of Shanghai University of Engineering Science (0234-E3-0903-19-01367).

References

[1] J.N. Zhao, F.L. Wang, X. Zhang, L.J. Liang, X.Q. Yang, Q.W. Li, X.H. Zhang, Vibration damping of carbon nanotube assembly materials, *Adv. Eng. Mater.* 20 (3) (2018) 1700647.
[2] N. Choudhary, D. Kaur, Vibration damping materials and their applications in nano/micro-electro-mechanical systems: A review, *J. Nanosci. Nanotechnol.* 15 (3) (2015) 1907–1924.
[3] J.L. Luo, Z.D. Duan, G.J. Xian, Q.Y. Li, T.J. Zhao, Damping performances of carbon nanotube reinforced cement composite, *Mech. Adv. Mater. Struct.* 22 (3) (2015) 224–232.
[4] W.M. van Spengen, MEMS reliability from a failure mechanisms perspective, *Microelectron. Reliab.* 43 (7) (2003) 1049–1060.
[5] C. Li, S.A. Xu, F.Y. Xiao, C.F. Wu, Dynamic mechanical properties of chlorinated butyl rubber blends, *Eur. Polym. J.* 42 (10) (2006) 2507–2514.
[6] D.W. Yang, X.Y. Zhao, T. Chan, L.Q. Zhang, S.Z. Wu, Investigation of the damping properties of hindered phenol AO-80/polyacrylate hybrids using molecular dynamics simulations in combination with experimental methods, *J. Mater. Sci.* 51 (12) (2016) 5760–5774.
[7] C. Su, D.Z. Zong, L.H. Xu, C. Zhang, Dynamic mechanical properties of semi-interpenetrating polymer network-based on nitrile rubber and poly(methyl methacrylate-co-butyl acrylate), *J. Appl. Polym. Sci.* 131 (9) (2014) 40217.
[8] L. Quiroga Cortes, L. Sanches, C. Bessaguet, M. Chevalier, C. Lacabanne, E. Dantras, G. Michon, Improving damping capabilities of composites structures by electroactive films containing piezoelectric and conductive fillers, *Smart Mater. Struct.* 30 (8) (2021) 085008.
[9] Z.Y. Sheng, J.C. Wang, S.Y. Yang, S.Q. Song, Novel polysiloxane microspheres: Preparation and application in chlorinated butyl rubber (CIIR) damping composites, *Adv. Powder Technol.* 30 (3) (2019) 632–643.
[10] J.Y. Liang, S.Q. Chang, N. Feng, Effect of C5 petroleum resin content on damping behavior, morphology, and mechanical properties of BIIR/BR vulcanizates, *J. Appl. Polym. Sci.* 130 (1) (2013) 510–515.
[11] F.S. Zhang, G.S. He, K.M. Xu, H. Wu, S.Y. Guo, The damping and flame-retardant properties of poly(vinyl chloride)/chlorinated butyl rubber multilayered composites, *J. Appl. Polym. Sci.* 132 (2) (2015) 41259.
[12] Z. Gu, L. Gao, G.J. Song, W.S. Liu, P.Y. Li, C.P. Shan, Octadecylammonium montmorillonite/natural rubber/*cis*-1,4-polybutadiene nanocomposites, *Appl. Clay Sci.* 50 (1) (2010) 143–147.
[13] X. Wang, D.L. Chen, W.S. Zhong, L. Zhang, X.Q. Fan, Z.B. Cai, M.H. Zhu, Experimental and theoretical evaluations of the interfacial interaction between carbon nanotubes and carboxylated butadiene nitrile rubber: Mechanical and damping properties, *Mater. Des.* 186 (2020) 108318.
[14] K.Y. Tang, J.C. Wang, Chlorinated butyl rubber/two-step modified montmorillonite nanocomposites: Mechanical and damping properties, *Chin. J. Chem. Eng.* 42 (2022) 437–449.
[15] L. Bokobza, Multiwall carbon nanotube elastomeric composites: A review, *Polymer* 48 (17) (2007) 4907–4920.
[16] X. Yu, Y. Zhang, L. Jin, J.Y. Chen, Z.H. Jiang, Y.H. Zhang, High-performance piezo-damping materials based on CNTs/$BaTiO_3$/F-PAEK-b-PDMS under high temperature steam conditions, *Appl. Surf. Sci.* 452 (2018) 429–436.
[17] C.H. Dai, X.J. Cao, K. Gou, Q.Y. Yin, B.J. Du, G.S. Weng, Iron (III) cross-linked thermoplastic nitrile butadiene elastomer with temperature-adaptable self-healing property, *J. Polym. Res.* 28 (3) (2021) 1–9.
[18] Z.X. Li, Y.F. Shan, X.X. Wang, H. Li, K. Yang, Y.Y. Cui, Self-healing flexible sensor based on metal-ligand coordination, *Chem. Eng. J.* 394 (2020) 124932.
[19] Y. Lu, J.C. Wang, L. Wang, S.Q. Song, Diphenolic acid-modified PAMAM/chlorinated butyl rubber nanocomposites with superior mechanical, damping, and self-healing properties, *Sci. Technol. Adv. Mater.* 22 (1) (2021) 14–25.
[20] C.F. Wu, Effects of a hindered phenol compound on the dynamic mechanical properties of chlorinated polyethylene, acrylic rubber, and their blend, *J. Appl. Polym. Sci.* 80 (13) (2001) 2468–2473.
[21] J.H. Zhang, C. Wang, W.T. Zao, H.D. Feng, Y.G. Hou, A.J. Huo, High-performance nitrile butadiene rubber composites with good mechanical properties, tunable elasticity, and robust shape memory behaviors, *Ind. Eng. Chem. Res.* 59 (36) (2020) 15936–15947.
[22] C. Su, P. He, R.J. Yan, C.B. Zhao, C. Zhang, Study of the orientation-controlled damping temperature based on selective distribution of oligo-phenol in acrylate rubber/chlorinated butyl rubber blends, *Polym. Compos.* 33 (6) (2012) 860–865.
[23] D.A. Tomalia, A.M. Naylor, W.A.I. Goddard, Starburst-dendrimere: Kontrolle von größe, gestalt, oberflächenchemie, topologie und flexibilität beim übergang von atomen zu makroskopischer materier, *Angew. Chem.* 102 (2) (1990) 119–157.
[24] Y.R. Lee, S.Q. Zhang, K. Yu, J. Choi, W.S. Ahn, Poly(amidoamine) dendrimer immobilized on mesoporous silica foam (MSF) and fibrous nano-silica KCC-1 for Gd^{3+} adsorption in water, *Chem. Eng. J.* 378 (2019) 122133.
[25] J. Manikkath, A. Manikkath, G.V. Shavi, K. Bhat, S. Mutalik, Low frequency ultrasound and PAMAM dendrimer facilitated transdermal delivery of ketoprofen, *J. Drug Deliv. Sci. Technol.* 41 (2017) 334–343.
[26] V.M. Thanh, T.H. Nguyen, T.V. Tran, U.-T.-P. Ngoc, M.N. Ho, T.T. Nguyen, Y.N.T. Chau, N.Q. Tran, C.K. Nguyen, D.H. Nguyen, Low systemic toxicity nanocarriers fabricated from heparin-mPEG and PAMAM dendrimers for controlled drug release, *Mater. Sci. Eng., C* 82 (2018) 291–298.
[27] G. Yang, D.L. Qing, H.F. Gao, N.P. Xu, Effect of the para-substituent of the tridentate pyridine-based Ru(II) complex upon the catalytic activity in transfer hydrogenation, *Chin. J. Chem. Eng.* 19 (1) (2011) 169–172.
[28] F. Giacalone, V. Campisciano, C. Calabrese, V. La Parola, Z. Syrgiannis, M. Prato, M. Gruttadauria, Single-walled carbon nanotube–polyamidoamine dendrimer hybrids for heterogeneous catalysis, *ACS Nano* 10 (4) (2016) 4627–4636.
[29] N.U. Kaya, F.E. Du Prez, N. Badi, Multifunctional dendrimer formation using thiolactone chemistry, *Macromol. Chem. Phys.* 218 (18) (2017) 1600575.

[30] S. Martens, J. Van den Begin, A. Madder, F.E. Du Prez, P. Espeel, Automated synthesis of monodisperse oligomers, featuring sequence control and tailored functionalization, *J. Am. Chem. Soc.* 138 (43) (2016) 14182–14185.
[31] C. Mertens, M. Soete, M.L. Ślęczkowski, A.R.A. Palmans, E.W. Meijer, N. Badi, F. E. Du Prez, Stereocontrolled, multi-functional sequence-defined oligomers through automated synthesis, *Polym. Chem.* 11 (26) (2020) 4271–4280.
[32] M.A. Meyers, J. McKittrick, P.Y. Chen, Structural biological materials: Critical mechanics-materials connections, *Science* 339 (6121) (2013) 773–779.
[33] C.H. Xu, J.D. Nie, W.C. Wu, L.H. Fu, B.F. Lin, Design of self-healable supramolecular hybrid network based on carboxylated styrene butadiene rubber and nano-chitosan, *Carbohydr. Polym.* 205 (2019) 410–419.
[34] C.H. Xu, W.C. Wu, J.D. Nie, L.H. Fu, B.F. Lin, Preparation of carboxylic styrene butadiene rubber/chitosan composites with dense supramolecular network via solution mixing process, *Compos. A Appl. Sci. Manuf.* 117 (2019) 116–124.
[35] P. Espeel, S. Celasun, P.S. Omurtag, S. Martens, F.E. Du Prez, Responsive thiolactone-derived N-substituted poly(urethane-amide)s, *Macromol. Rapid Commun.* 38 (7) (2017) 1600783.
[36] Y. Motoyama, K. Kamo, H. Nagashima, Catalysis in polysiloxane gels: Platinum-catalyzed hydrosilylation of polymethylhydrosiloxane leading to reusable catalysts for reduction of nitroarenes, *Org. Lett.* 11 (6) (2009) 1345–1348.
[37] A.L. Sun, W.J. Guo, J.P. Zhang, W.J. Li, X. Liu, H. Zhu, Y.H. Li, L.H. Wei, Excellent toughening of 2,6-diaminopyridine derived poly (urethane urea) via dynamic cross-linkages and interfering with hydrogen bonding of urea groups from partially coordinated ligands, *Polymers* 11 (8) (2019) 1320.
[38] Z.H. Tang, X.H. Wu, B.C. Guo, L.Q. Zhang, D.M. Jia, Preparation of butadiene–styrene–vinyl pyridine rubber–graphene oxide hybrids through co-coagulation process and in situ interface tailoring, *J. Mater. Chem.* 22 (15) (2012) 7492–7501.
[39] Z.H. Tang, J. Huang, B.C. Guo, L.Q. Zhang, F. Liu, Bioinspired engineering of sacrificial metal-ligand bonds into elastomers with supramechanical performance and adaptive recovery, *Macromolecules* 49 (5) (2016) 1781–1789.
[40] M. Hayashi, S. Matsushima, A. Noro, Y. Matsushita, Mechanical property enhancement of ABA block copolymer-based elastomers by incorporating transient cross-links into soft middle block, *Macromolecules* 48 (2) (2015) 421–431.
[41] L.A. Saghatforoush, A. Aminkhani, S. Ershad, G. Karimnezhad, S. Ghammamy, R. Kabiri, Preparation of zinc (II) and cadmium (II) complexes of the tetradentate Schiff base ligand 2-((E)-(2-(2-(pyridine-2-yl)-ethylthio)ethylimino)methyl)-4-bromophenol (PytBrsalH), *Molecules* 13 (4) (2008) 804–811.
[42] Y. Chen, Z.H. Tang, Y.J. Liu, S.W. Wu, B.C. Guo, Mechanically Robust, Self-healable, and reprocessable elastomers enabled by dynamic dual cross-links, *Macromolecules* 52 (10) (2019) 3805–3812.
[43] M.W. Yan, L.M. Cao, C.H. Xu, Y.K. Chen, Fabrication of "Zn^{2+} salt-bondings" cross-linked SBS-g-COOH/ZnO composites: Thiol–ene reaction modification of SBS, structure, high modulus, and shape memory properties, *Macromolecules* 52 (11) (2019) 4329–4340.
[44] D. Mozhdehi, S. Ayala, O.R. Cromwell, Z.B. Guan, Self-healing multiphase polymers *via* dynamic metal-ligand interactions, *J. Am. Chem. Soc.* 136 (46) (2014) 16128–16131.
[45] F.S. Zhang, G.S. He, K.M. Xu, H. Wu, S.Y. Guo, C.L. Zhang, Damping mechanism and different modes of molecular motion through the glass transition of chlorinated butyl rubber and petroleum resin blends, *J. Appl. Polym. Sci.* 131 (13) (2014) 40464.
[46] C. Liu, J.F. Fan, Y.K. Chen, Design of regulable chlorobutyl rubber damping materials with high-damping value for a wide temperature range, *Polym. Test.* 79 (2019) 106003.
[47] Z.X. Gu, A.J. Xu, J.B. Chang, S.W. Li, Y.B. Xiang, Optimization of the production organization pattern in Tangshan Iron and Steel Co., Ltd, *J. Iron Steel Res. Int.* 21 (2014) 17–22.
[48] F. Song, Z.S. Li, P.Y. Jia, M. Zhang, C.Y. Bo, G.D. Feng, L.H. Hu, Y.H. Zhou, Tunable "soft and stiff", self-healing, recyclable, thermadapt shape memory biomass polymers based on multiple hydrogen bonds and dynamic imine bonds, *J. Mater. Chem. A* 7 (21) (2019) 13400–13410.
[49] J. Cao, C.H. Lu, J. Zhuang, M.X. Liu, X.X. Zhang, Y.M. Yu, Q.C. Tao, Multiple hydrogen bonding enables the self-healing of sensors for human-machine interactions, *Angew. Chem. Int. Ed.* 56 (30) (2017) 8795–8800.